IEEE Photonics Journal
An IEEE Photonics Society Publication

Open Access

FSR-Eliminated Vernier Racetrack Resonators Using Grating-Assisted Couplers

Volume 5, Number 5, October 2013

R. Boeck, Student Member, IEEE
W. Shi, Member, IEEE
L. Chrostowski, Member, IEEE
N. A. F. Jaeger, Member, IEEE

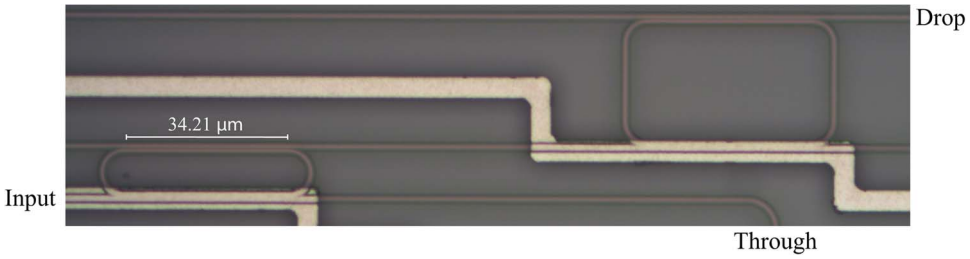

DOI: 10.1109/JPHOT.2013.2280342
1943-0655 © 2013 IEEE

IEEE photonics SOCIETY

IEEE

FSR-Eliminated Vernier Racetrack Resonators Using Grating-Assisted Couplers

R. Boeck,[1] *Student Member, IEEE*, W. Shi,[2] *Member, IEEE*, L. Chrostowski,[1] *Member, IEEE*, and N. A. F. Jaeger,[1] *Member, IEEE*

[1]Department of Electrical and Computer Engineering, The University of British Columbia, Vancouver, BC V6T 1Z4, Canada
[2]Department of Electrical and Computer Engineering and the Center for Optics, Photonics, and Lasers (COPL), Université Laval, Québec, QC G1V0A6, Canada

DOI: 10.1109/JPHOT.2013.2280342

Manuscript received June 20, 2013; revised August 16, 2013; accepted August 16, 2013. Date of publication August 30, 2013; date of current version September 10, 2013. This work was supported in part by the Natural Sciences and Engineering Research Council of Canada under the CREATE SiEPIC, Discovery Grants, and Postgraduate Programs. Part of this work was conducted at the University of Washington Microfabrication Facility, a member of the NSF National Nanotechnology Infrastructure Network. Corresponding author: R. Boeck (e-mail: rboeck@ieee.org).

Abstract: We present the design and experimental demonstration of a contra-directional grating-coupled racetrack resonator exhibiting the Vernier effect. The device consists of two racetrack resonators that are coupled together in a cascaded configuration. The input coupler in each racetrack resonator of the cascaded configuration consists of contra-directional gratings. The benefit of using contra-directional couplers is their small bandwidth, as compared to co-directional couplers that do not have gratings. The simulation results show that this device provides numerous performance advantages compared to cascaded racetrack resonators exhibiting the Vernier effect without contra-directional grating couplers. Specifically, we eliminate the free spectral range (FSR, i.e., in both the drop port and the through port) and show substantial improvement in the interstitial peak suppression and the through port insertion loss for the cascaded racetrack resonator with gratings, as compared to the case without gratings. In addition, experimental results are presented, which show an interstitial peak suppression of 29.3 dB, as well as the elimination of the FSR in the drop port and the through port.

Index Terms: Silicon nanophotonics, gratings, waveguide devices.

1. Introduction

Cascaded racetrack resonators exhibiting the Vernier effect have numerous benefits compared to single racetrack resonators, including an extended free spectral range (FSR) in the drop port [1]–[7]. However, the through port spectral response does not have an increased FSR [1], [7], which can be problematic for certain dense wavelength-division multiplexing (DWDM) applications. Fortunately, series-coupled racetrack resonators can exhibit the Vernier effect in both the drop port and the through port [1], [8], [9]. Numerous papers have presented theoretical [10]–[15] results as well as experimental [4], [8], [9], [16]–[22] results for series-coupled Vernier resonators consisting of two [4], [8], [11]–[14], [16], [18]–[22], three [11]–[13], [15], [17], and four [9], [10], [13]–[15] rings. Also, combinations of cascaded and series-coupled Vernier ring resonators have been theoretically analyzed [23]. Recently, Yan *et al.* [24] presented a novel configuration of microring resonators exhibiting the Vernier effect in which one ring resonator is directly coupled to four smaller ring

resonators. Also, Vernier ring resonators have been used to create sensors [25]–[28] and tunable lasers [29], [30]. Due to fabrication variations, the performance of the ring resonators may be significantly degraded. Thermal tuning of each individual ring resonator is needed to correct for the fabrication variations. A benefit of the cascaded configuration of ring resonators, as compared to the series-coupled configuration, is that the thermal cross-talk between resonators is reduced due to the increased distance between the rings [2]. Recently, Shi *et al.* [31] designed and fabricated a new single racetrack resonator with contra-directional gratings within the coupling regions to suppress all but a single resonance in the drop port and the through port, which is due to the small bandwidth of the coupler. The suppression of minor peaks is greater than 8 dB [31]. Orlandi *et al.* [32] presented experimental results on a racetrack resonator with gratings within the coupling regions but their device showed minimal suppression of peaks in the drop port. Also, Orlandi *et al.* [32] discussed and presented theoretical results on a modified version of their grating coupled racetrack resonator in which the input coupler has gratings but the output coupler does not. In this paper, we demonstrate both theoretically and experimentally contra-directional grating-coupled cascaded racetrack resonators exhibiting the Vernier effect. The theoretical results show the elimination of the FSR (in both the drop port and the through port) as well as the improvement in the interstitial peak suppression, IPS, at the drop port and the improvement in the through port insertion loss, IL_{thru}, as compared to the case in which no gratings were used. Our fabricated device shows an improvement in the suppression of minor peaks in the drop port as compared to the suppression shown by [31] and [32]. Our experimental results show an IPS of 29.3 dB and the elimination of the FSR in the drop port and through port.

2. Theory

We have decided to use silicon-on-insulator (SOI) strip waveguides with a top oxide cladding for the FSR-eliminated grating-coupled cascaded Vernier racetrack resonator, since previous experimental results by Shi *et al.* [31] have shown promising results for individual grating-coupled racetrack resonators. The waveguide heights are 220 nm and the bus waveguide widths, w_b, and the racetrack resonator widths, w_r, are 450 nm and 550 nm, respectively. For the coupling regions that have co-directional coupling (no gratings), w_b and w_r are 550 nm and the gap distance is 280 nm. The gratings within the coupling regions are formed by corrugating the sidewalls as shown in Fig. 1(a). The corrugation depths, c_b and c_r, for waveguides with widths of w_b and w_r, are defined as the extensions into the waveguides by $c_b/2$ and $c_r/2$ and into the gap by $c_b/2$ and $c_r/2$. The number of grating periods, P, is 110 and the perturbation period, Λ, is 311 nm, such that the drop port peak wavelength, λ_D, is very close to the resonance wavelength, λ_r, which corresponds to the major peak within the drop port spectrum of the cascaded Vernier racetrack resonator. The contra-directional grating coupler was designed so that the value of the contra-directional power coupling factor, $|\kappa_c|^2$, and the contra-directional power transmission factor, $|t_c|^2$, would be very close to the value of the co-directional power coupling factor, $|\kappa|^2$, and power transmission factor, $|t|^2$, at λ_D when the losses in the couplers are taken into account. In order to suppress Bragg reflections back to the input port, an anti-reflection grating structure has been used, where additional gratings are formed on the external side-walls of the coupler [33] as shown in Fig. 1(a). These external grating are out of phase with respective to the gratings inside the coupler region, which can significantly suppress back reflections through destructive interference [33].

The schematic of the grating-coupled cascaded Vernier racetrack resonator is shown in Fig. 1(b), where; "a" is the first racetrack, "b" is the second (larger) racetrack, and "tr" is the tapered routing section between the resonators, $Z_{a,b,\mathrm{tr}}(\lambda) = \exp(-\alpha_{a,b,\mathrm{tr}} L_{a,b,\mathrm{tr}} - j\beta_{a,b,\mathrm{tr}}(\lambda) L_{a,b,\mathrm{tr}})$, $\beta_{a,b,\mathrm{tr}}(\lambda) = 2\pi n_{\mathrm{eff\_}a,b,\mathrm{tr}}(\lambda)/\lambda$, $n_{\mathrm{eff\_}a,b,\mathrm{tr}}(\lambda)$ is the appropriate waveguide effective index, L_a and L_b are the total lengths of the racetrack resonators neglecting the lengths of the straight coupling regions, and $\alpha_a[\mathrm{m}^{-1}]$ and $\alpha_b[\mathrm{m}^{-1}]$ are the total field loss coefficients. L_{tr} and α_{tr} are the length and field loss coefficient of the tapered routing section between the two racetrack resonators. $\kappa_1(\lambda)$ and $\kappa_3(\lambda)$ are the symmetric complex field contra-directional coupling factors of the grating couplers of racetrack resonators "a" and "b". $t_1(\lambda)$ and $t_3(\lambda)$ are the straight-through racetrack waveguide complex field

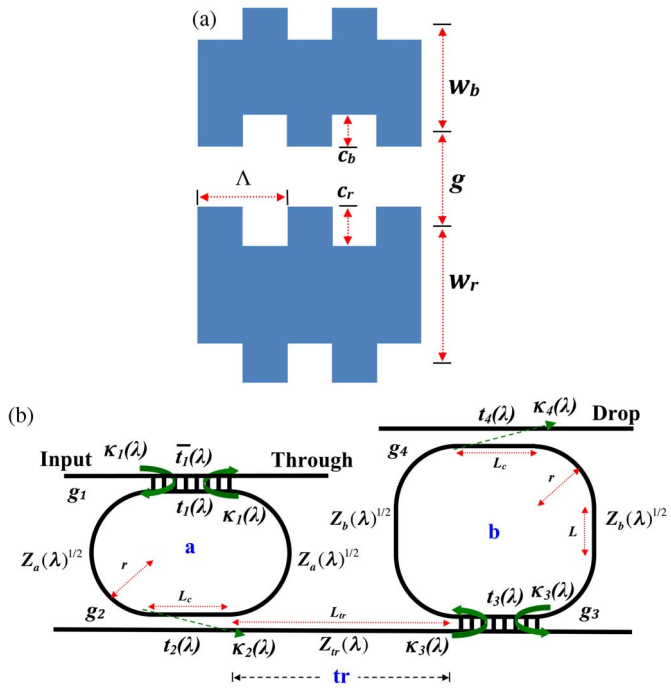

Fig. 1. (a) Schematic of a section of the contra-directional grating coupler and (b) schematic of the grating-coupled cascaded Vernier racetrack resonator.

transmission factors of the grating couplers of racetrack resonators "a" and "b". $\bar{t}_1(\lambda)$ is the straight-through bus waveguide complex field transmission factor of the grating coupler of racetrack resonator "a". The propagation constant in the expression for $\bar{t}_1(\lambda)$ is different from that in the expression for $t_1(\lambda)$ since the bus waveguide and racetrack resonator widths are different. $\kappa_2(\lambda)$ and $\kappa_4(\lambda)$ are the symmetric complex field co-directional coupling factors of the waveguides. $t_2(\lambda)$ and $t_4(\lambda)$ are the straight-through complex field transmission factors of the waveguides.

The drop port and through port intensity responses of the grating-coupled cascaded Vernier racetrack resonator can be determined by multiplying Eq. (1) and Eq. (2) by their respective complex conjugates,

$$E_{\text{Drop}}(\lambda) = \frac{\kappa_1(\lambda)\kappa_2(\lambda)Z_a(\lambda)^{1/2}}{1 - t_1(\lambda)t_2(\lambda)Z_a(\lambda)} \times Z_{\text{tr}}(\lambda) \times \frac{\kappa_3(\lambda)\kappa_4(\lambda)Z_b(\lambda)^{1/2}}{1 - t_3(\lambda)t_4(\lambda)Z_b(\lambda)}, \tag{1}$$

$$E_{\text{Through}}(\lambda) = \frac{\kappa_1(\lambda)^2 t_2(\lambda)Z_a(\lambda) + \bar{t}_1(\lambda)(1 - t_1(\lambda)t_2(\lambda)Z_a(\lambda))}{1 - t_1(\lambda)t_2(\lambda)Z_a(\lambda)} \tag{2}$$

where,

$$\kappa_1(\lambda) = \kappa_3(\lambda) = \kappa_c(\lambda), \tag{3}$$

$$t_1(\lambda) = t_3(\lambda) = t_c(\lambda)e^{-j\beta_{a,b}(\lambda)L_c - \alpha_{a,b}L_c}, \tag{4}$$

$$\bar{t}_1(\lambda) = t_c(\lambda)e^{-j\bar{\beta}_a(\lambda)L_c - \bar{\alpha}_a L_c}, \tag{5}$$

$$\kappa_2(\lambda) = \kappa_4(\lambda) = -j\sin\left(\frac{\pi L_c}{2L_\pi(\lambda)}\right)e^{-j\beta_{a,b}(\lambda)L_c - \alpha_{a,b}L_c}, \tag{6}$$

$$t_2(\lambda) = t_4(\lambda) = \cos\left(\frac{\pi L_c}{2L_\pi(\lambda)}\right)e^{-j\beta_{a,b}(\lambda)L_c - \alpha_{a,b}L_c}. \tag{7}$$

The following design was chosen for all simulations: $L_a = 2\pi r$, where $r = 4.65$ μm, and $L_c = \Lambda \times P$ where Λ and P are 311 nm and 110, respectively, $L_b = 2\pi r + 2L$, where $L = 16.27$ μm, β_a

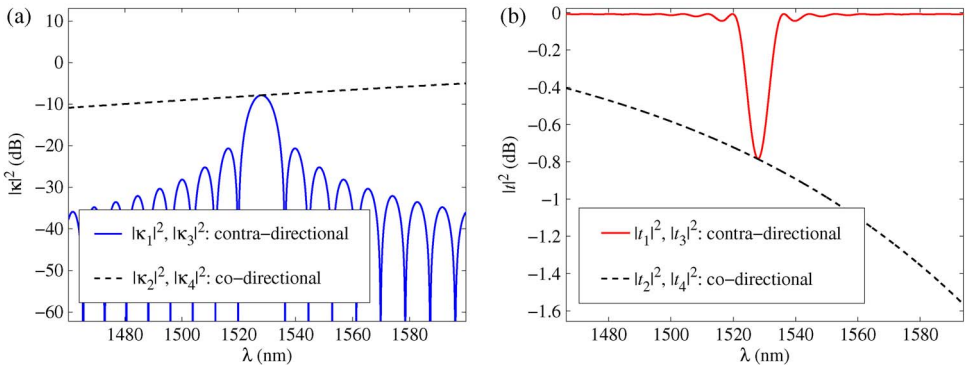

Fig. 2. (a) $|\kappa|^2$ versus λ for the contra-directional (blue-solid) and co-directional (black-dash) couplers. (b) $|t|^2$ versus λ for the contra-directional (red-solid) and co-directional (black-dash) couplers.

and β_b are for waveguide widths of 550 nm, $\overline{\beta_a}$ is for a waveguide width of 450 nm, and $L_\pi(\lambda)$ is the cross-over length. It should be noted that the ratio of the total length of resonator "b" to the total length of resonator "a" was chosen to be 4/3. Also, we assume that the propagation constants for the two racetrack resonators are identical (i.e., the effective index is the same for all regions of each racetrack). The propagation loss seen from the input port to the through port, $\overline{\alpha_a}[\mathrm{m}^{-1}]$, is 7.4 dB/cm [34], since the waveguide width is 450 nm. Also, the propagation loss for each ring is assumed to be 2 dB/cm, since their waveguide widths are 550 nm. We assume the optical attenuation due to the routing section between the two racetrack resonators is minimal and therefore the routing section is not included in our calculations. Finally, it is assumed that, since the waveguides within the coupling regions with gratings have different propagation constants, the co-directional coupling is minimal and is neglected in the model. In other words, only contra-directional coupling is considered within the regions with gratings.

To determine the complex field contra-directional coupling factors and the straight-through complex field transmission factors of the gratings, the modeling method presented by Shi *et al.* was used [31], [35]. Here, we have chosen the coupling coefficient to be 12551 m^{-1} so that the contra-directional power coupling and power transmission factors are close to the values of the co-directional power coupling and power transmission factors at λ_D. To determine the symmetric complex field co-directional coupling and transmission factors, $L_\pi(\lambda)$ was determined using a numerical mode solver. The effective indices of the co-directional couplers and the waveguides were calculated at 11 wavelengths between 1500 nm and 1600 nm and curve-fitted to third-order polynomials from which all effective indices were obtained. Fig. 2(a) and (b) show the wavelength dependent contra-directional and co-directional power coupling factors and the straight-through power transmission factors for the coupler with and without gratings.

Fig. 3(a) shows the drop port responses for two independent single contra-directional grating-coupled racetrack resonators with lengths L_a (green-solid) and L_b (red-dash). The limited suppression of the peaks to the left and to the right of the major peaks for the single racetrack resonators are due to the bandwidth of the contra-directional grating couplers. Fig. 3(b) shows the drop port responses for the cascaded configuration of these two racetrack resonators with (blue-solid) and without (black-dash) gratings. In the case where there are no gratings, we change the structure shown in Fig. 1(b) such that the input port and the through port are exchanged with each other as well as the drop port being placed at the spare output port. We can clearly see that the grating-coupled cascaded Vernier racetrack resonator spectrum shows increased suppression of all minor peaks as compared to the spectra of the other three devices. However, we also need to compare the response of the grating-coupled cascaded Vernier racetrack resonator to that of a grating-coupled cascaded identical racetrack resonator with lengths L_a as well as L_b. Fig. 3(c) shows the drop port responses for grating-coupled cascaded Vernier (blue-solid) racetrack resonators as well as the response for identical (orange-dash) racetrack resonators with lengths L_a. Fig. 3(d) shows the drop port responses for grating-coupled cascaded Vernier (blue-solid) racetrack resonators as

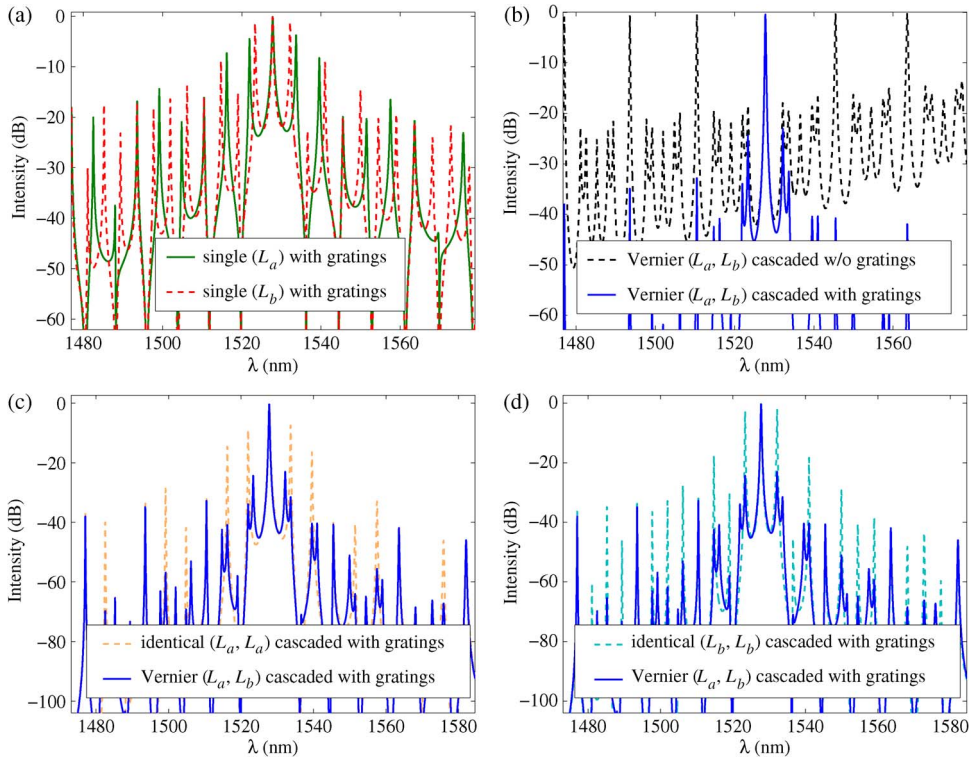

Fig. 3. (a) Drop port spectral response comparison between single grating-coupled racetrack resonator with length L_a (green-solid) and L_b (red-dash), (b) coupled Vernier racetrack resonator with (blue-solid) and without (black-dash) contra-directional grating couplers, (c) drop port spectral response comparison between grating-coupled cascaded identical racetrack resonator with lengths L_a and grating-coupled cascaded Vernier racetrack resonator, and (d) drop port spectral response comparison between grating-coupled cascaded identical racetrack resonator with lengths L_b and grating-coupled cascaded Vernier racetrack resonator.

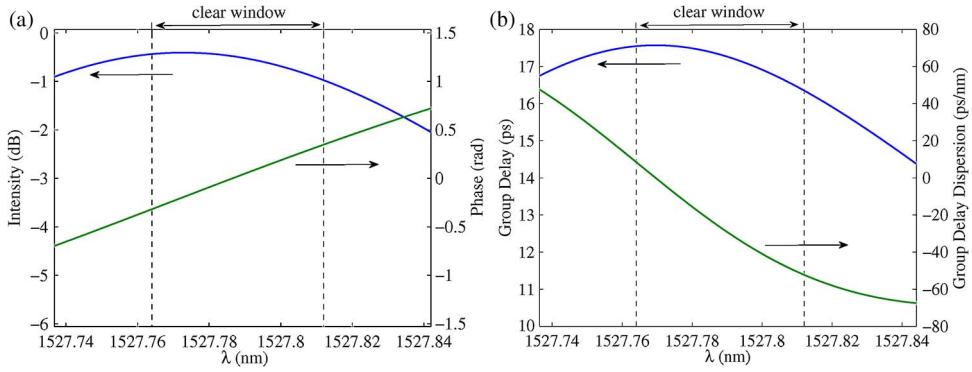

Fig. 4. (a) Drop port spectral response and phase and (b) group delay and group delay dispersion of our grating-coupled cascaded Vernier racetrack resonator.

well as the response for identical (light blue-dash) racetrack resonators with lengths L_b. In both cases, the Vernier effect causes an increase in suppression of all minor peaks as compared to the cases where identical racetrack resonators were used. The drop port spectrum and phase in the vicinity of the clear window of our grating-coupled cascaded Vernier racetrack resonator are shown in Fig. 4(a). The group delay and the group delay dispersion (or chromatic dispersion) of our grating-coupled cascaded Vernier racetrack resonator are shown in Fig. 4(b). Next, we compare the

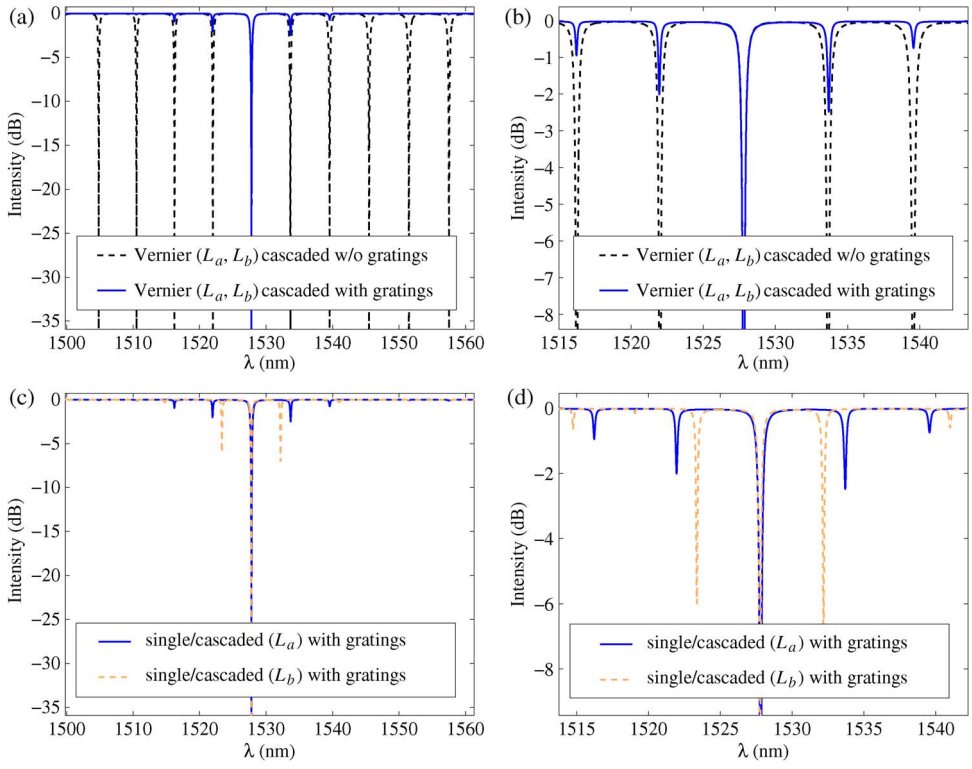

Fig. 5. (a) Through port spectral response comparison between grating-coupled cascaded Vernier racetrack resonator (blue-solid) and cascaded Vernier racetrack resonator without gratings (black-dash), (b) a "zoom-in" of the major notch in Fig. 5(a), (c) through port spectral response comparison between grating-coupled single (response same as cascaded configuration) racetrack resonator with lengths L_a and L_b, and (d) a "zoom-in" of the major notch in Fig. 5(c).

through port response for cascaded Vernier racetrack resonators with and without gratings, as shown in Fig. 5(a) and (b). We can clearly see that using gratings is beneficial, since it significantly suppresses all but one of the resonances. The through port response for the grating-coupled cascaded identical racetrack resonator has the same response as that of a single contra-directional grating-coupled racetrack resonator when its dimensions are the same as one of the racetrack resonators in the cascaded configuration. In Fig. 5(c) and (d), the through port responses for grating-coupled cascaded (single) identical racetrack resonator with lengths L_a as well as L_b are shown. It can be clearly seen that the response for the device with lengths L_a has more suppression of its minor notches as compared to the device with lengths L_b.

All specifications are defined for a channel spacing of 0.8 nm, a clear window of 0.048 nm, and within the clear window of channel x as well as the clear windows of the 44 channels to the left and to the right of channel x (the number of channels within the ITU grid for the C-band is 45 [36]). Here, the clear window is centered at a wavelength value corresponding to the average wavelength value of the major peak between its -3 dB points and -20 dB points (referenced at the maximum intensity of the major peak) and of the major notch between its -3 dB points and -20 dB points (referenced at the maximum intensity of the major notch). It should be noted that we have assumed that the clear window has the same definition as the channel wavelength range which is defined by the ITU [37], [38]. The drop port adjacent channel isolation, A_i, is defined as the difference (in dB) between the minimum transmission of the filter within the clear window of channel x and the maximum transmission of the filter within the clear windows of adjacent channels $x - 1$ and $x + 1$ [37]. The non-adjacent channel isolation, nA_i, is the difference (in dB) between the minimum transmission within the clear window of the operating channel and the maximum transmission within the clear windows of all non-adjacent channels [37]. It should be noted that the IPS has the same definition as nA_i. The

TABLE 1

Drop port and through port insertion loss for single racetrack resonators with gratings, cascaded Vernier racetrack resonators with and without gratings, and grating-coupled cascaded identical racetrack resonators

Parameter	single (L_a) with gratings	single (L_b) with gratings	cascaded Vernier w/o gratings	cascaded identical (L_a) with gratings	cascaded identical (L_b) with gratings	cascaded Vernier with gratings
IL_{drop} (dB)	0.3	0.5	1.0	0.4	0.6	1.0
IL_{thru} (dB)	0.3	0.3	8.8	0.3	0.2	0.3

TABLE 2

Spectral characteristics for single racetrack resonators with gratings, cascaded Vernier racetrack resonators with and without gratings, and grating-coupled cascaded identical racetrack resonators

Parameter	single (L_a) with gratings	single (L_b) with gratings	cascaded Vernier w/o gratings	cascaded identical (L_a) with gratings	cascaded identical (L_b) with gratings	cascaded Vernier with gratings
FSR (nm)	N/A	N/A	5.81, 5.85	N/A	N/A	N/A
A_i (dB)	12.9	15.1	27.8	26.0	30.3	27.9
nA_i, IPS (dB)	11.3	12.5	0.1	23.6	25.8	33.9
R_{depth} (dB)	0.2	0.3	0.6	0.2	0.3	0.6
EC_i (dB)	12.8	11.1	13.7	16.5	14.4	13.8

drop port insertion loss, IL_{drop}, or channel insertion loss, is defined as the minimum transmission within the clear window of channel x [36], [37]. The difference between the maximum drop port transmission and the IL_{drop} within the clear window of channel x is termed the ripple, R_{depth}, [36], [37]. The express channel isolation, EC_i, or channel extinction, of the through port is the value of the difference in transmission between the minimum transmission within the clear window of all adjacent channels and non-adjacent channels and the maximum transmission within the clear window of channel x [37]. However, here we will only define the minimum transmission within the adjacent channels when determining the EC_i, which is in agreement with the definition for the pass channel residual at express port found in [39]. The maximum through port insertion loss, IL_{thru}, is defined as the minimum transmission within the clear windows of all adjacent and non-adjacent channels.

Tables 1 and 2 show the spectral characteristics of the single grating-coupled racetrack resonators with lengths L_a and L_b, the cascaded Vernier racetrack resonator with and without contra-directional gratings, and of the grating-coupled cascaded identical racetrack resonators. We can clearly see that the cascaded Vernier racetrack resonator with gratings shows a significant improvement in its FSR (in fact, there is no FSR), IPS, and IL_{thru} as compared to the response of the cascaded racetrack resonator without gratings. In the case of the cascaded configuration without gratings, the drop port shows an extended FSR of 17.30 nm and 17.70 nm to the left and right of the major peak, respectively, whereas the through port response only shows an FSR of 5.81 nm and 5.85 nm. However, the inclusion of the contra-directional gratings removes the FSR in both the drop port and the through port. Also, the grating-coupled cascaded Vernier racetrack resonator shows significant improvements in its A_i and IPS as compared to both of the single contra-directional grating-coupled racetrack resonator responses. Also, the grating-coupled cascaded Vernier racetrack resonator shows an improvement in the IPS as compared to the responses of grating-coupled cascaded identical racetrack resonators. Thus, we can see the combined benefit of using contra-directional grating couplers and the Vernier effect within coupled racetrack resonators.

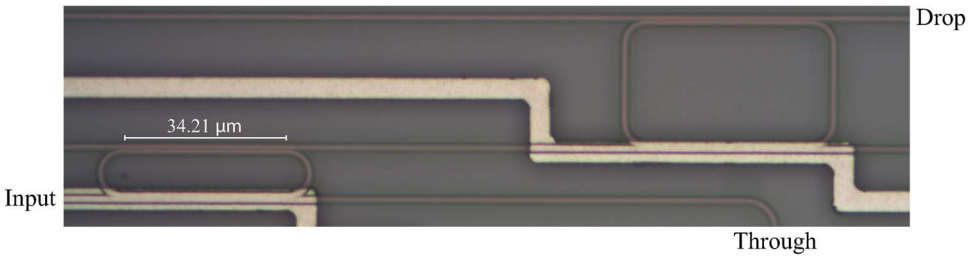

Fig. 6. Optical microscope image of the fabricated device.

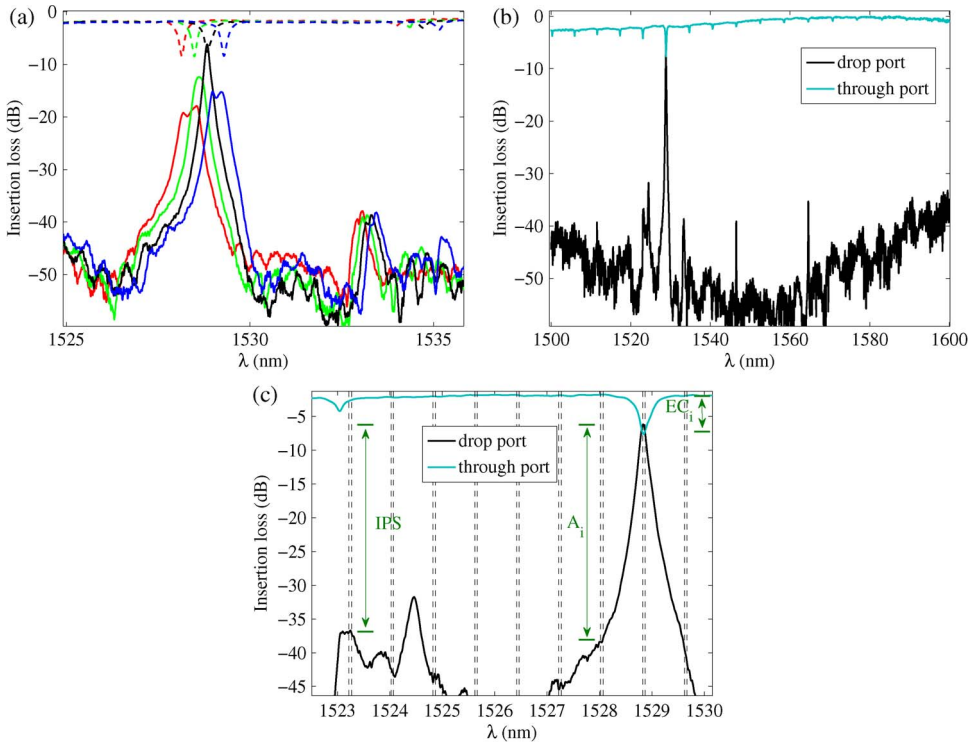

Fig. 7. (a) Experimental drop port (solid) and through port (dashed) responses when the voltage to the heater for racetrack resonator "a" is 0 V (red), 4V (green), 5.8 V (black), and 7 V (blue). (b) The experimental drop port (black) and through port (light blue) spectra when a voltage of 5.8 V is applied to the heater of racetrack resonator "a". (c) A zoom-in of Fig. 7(b) with a 0.048 nm clear window and 0.8 nm channel spacing indicated by the dashed vertical lines.

3. Experimental Results

The device was fabricated using e-beam lithography [40] at the University of Washington and aluminum (300 nm thick) metallization for the heaters (5 μm wide) and electrodes was done at McMaster University. Fig. 6 shows a microscope image of our device. Heaters were placed on each contra-directional coupling region to enable resonance tuning to correct for fabrication variations. The top oxide is 2 μm thick, the co-directional and contra-directional gap distances are 280 nm and 220 nm, w_b and w_r are 450 nm and 550 nm, the corrugation depths, c_b and c_r, for waveguides with widths of w_b and w_r are 30 nm and 40 nm, respectively. The tapered routing waveguide between the two racetrack resonators has a length of 74.912 μm.

Fig. 7(a) shows the experimental drop port and through port responses for applied voltages of 0 V, 4 V, 5.8 V, and 7 V to the contra-directional coupling region of racetrack resonator "a". We can clearly see that applying a voltage of 5.8 V significantly improves the major peak of the drop port response; the maximum drop port peak intensity increases from -17.9 dB to -6.2 dB. Fig. 7(b)

TABLE 3
Experimental results of grating-coupled cascaded Vernier racetrack resonator

Parameter	Measured value
FSR (nm)	N/A
A_i (dB)	30.5
nA_i, IPS (dB)	29.3
R_{depth} (dB)	1.2
EC_i (dB)	5.2

shows the through port and drop port responses for this case. The drop port response has one major peak and all other peaks are suppressed and the through port response shows one major notch and all other notches have smaller notch depths (less than 2 dB) as compared to the depth of the major notch (5.9 dB). Thus we have experimentally confirmed that it is possible to eliminate the FSR in the drop port and through port. Next, we determine the A_i, IPS, R_{depth}, and EC_i for a clear window of 0.048 nm centered at a wavelength of 1528.846 nm and a channel spacing of 0.8 nm. It should be noted that the minimum wavelength we measured the spectrum for is 1500 nm so only 36 channels to the left and 44 channels to the right of the desired channel were used in calculating the IPS. Fig. 7(c) shows a "zoom-in" of Fig. 7(b) which includes vertical dashed lines that represent the clear window and channel spacing as well as labels for A_i, IPS, and EC_i. Table 3 shows the experimental spectral characteristics of the grating-coupled cascaded Vernier racetrack resonator. The response of our device has no FSR in both the drop port and through port, which is in agreement with the theoretical result shown in Table 2 (we were unable to accurately determine the values for IL_{drop} and IL_{thru}). Also, the device has a large IPS of 29.3 dB (however, if a channel was centered on the minor peak located at 1524.465 nm, the IPS would be reduced to 24.3 dB). Our grating-coupled cascaded Vernier racetrack resonator needs further improvement to give a value of the EC_i that is greater than or equal to 10 dB [41], of the R_{depth} that is less than or equal to 0.5 dB [41], and of the IPS that is greater than or equal to 35 dB [42], so that this type of device can be used in typical DWDM applications. It should be noted that our device has an A_i of 30.5 dB (which is better than the 25 dB that can be found in data sheets for some commercial products [41]).

4. Conclusion

In summary, we have shown that using contra-directional couplers in cascaded racetrack resonators exhibiting the Vernier effect provides numerous advantages as compared to the responses of cascaded racetrack resonators exhibiting the Vernier effect without contra-directional gratings. The grating-coupled cascaded Vernier racetrack resonator studied here has a theoretical IPS and an IL_{thru} of 33.9 dB and 0.3 dB, respectively, whereas without the gratings the IPS is 0.1 dB and the IL_{thru} is 8.8 dB. The reason why the IL_{thru} is substantially improved is due to the suppression of all but one of the resonances in the through port, which is the result of the small bandwidth of the contra-directional grating coupler. Also, there is no FSR in both the drop port and through port for the grating-coupled cascaded Vernier racetrack resonator whereas there is a 17.30 nm/17.70 nm extended FSR at the drop port and an FSR of 5.81 nm/5.85 nm at the through port for the case without gratings. Also, we have presented experimental results which show that it is in fact possible to eliminate the FSR in the drop port as well as the through port. Our fabricated device also shows a large IPS of 29.3 dB. Thus, we are now able to use the cascaded configuration of the Vernier effect and not be limited to applications that only require a large FSR in the drop port.

Acknowledgment

We acknowledge CMC Microsystems, Mentor Graphics, and Lumerical Solutions, Inc., for access to the CAD tools used. We thank Y. Wang for the fiber grating coupler design. Also, we thank J. Flueckiger and C. Lin for the experimental setup and A. Kulpa for the optical microscope image. We would also like to thank E. Huante-Ceron and A. Knights at McMaster University for the metallization.

References

[1] E. J. Klein, "Densely integrated microring-resonator based components for fiber-to-the-home applications," Ph.D. dissertation, Univ. Twente, Enschede, The Netherlands, Apr. 2007.

[2] P. Prabhathan, Z. Jing, V. Murukeshan, Z. Huijuan, and C. Shiyi, "Discrete and fine wavelength tunable thermo-optic WSS for low power consumption $C + L$ band tunability," *IEEE Photon. Technol. Lett.*, vol. 24, no. 2, pp. 152–154, Jan. 2012.

[3] S. Chu, B. Little, V. Van, J. Hryniewicz, P. Absil, F. Johnson, D. Gill, O. King, F. Seiferth, M. Trakalo, and J. Shanton, "Compact full C-band tunable filters for 50 GHz channel spacing based on high order micro-ring resonators," presented at the Optical Fiber Communication Conference, Los Angeles, CA, USA, Feb. 2004, PDP 9.

[4] B. Timotijevic, G. Mashanovich, A. Michaeli, O. Cohen, V. M. N. Passaro, J. Crnjanski, and G. T. Reed, "Tailoring the spectral response of add/drop single and multiple resonators in silicon-on-insulator," *Chin. Opt. Lett.*, vol. 7, no. 4, pp. 291–295, Apr. 2009.

[5] S.-J. Choi, Z. Peng, Q. Yang, S. J. Choi, and P. D. Dapkus, "Tunable narrow linewidth all-buried heterostructure ring resonator filters using Vernier effects," *IEEE Photon. Technol. Lett.*, vol. 17, no. 1, pp. 106–108, Jan. 2005.

[6] G. Ren, T. Cao, and S. Chen, "Design and analysis of a cascaded microring resonator-based thermo-optical tunable filter with ultralarge free spectrum range and low power consumption," *Opt. Eng.*, vol. 50, no. 7, pp. 074601–074601-6, Jul. 2011. [Online]. Available: http://dx.doi.org/10.1117/1.3602879

[7] X. Zhang, L. Zhou, L. Lu, J. Xie, X. Sun, X. Li, and J. Chen, "Tunable Vernier microring optical filters using p-i-p resistor-based micro-heaters," presented at the Optical Fiber Communication Conference, Anaheim, CA, USA, Mar. 2013, Paper OTu3C.7 [Online]. Available: http://www.opticsinfobase.org/abstract.cfm?URI=OFC-2013-OTu3C.7

[8] W. S. Fegadolli, G. Vargas, X. Wang, F. Valini, L. A. M Barea, J. E. B. Oliveira, N. Frateschi, A. Scherer, V. R. Almeida, and R. R. Panepucci, "Reconfigurable silicon thermo-optical ring resonator switch based on Vernier effect control," *Opt. Exp.*, vol. 20, no. 13, pp. 14 722–14 733, Jun. 2012. [Online]. Available: http://www.opticsexpress.org/abstract.cfm?URI=oe-20-13-14722

[9] R. Boeck, J. Flueckiger, L. Chrostowski, and N. A. F. Jaeger, "Experimental performance of DWDM quadruple Vernier racetrack resonators," *Opt. Exp.*, vol. 21, no. 7, pp. 9103–9112, Apr. 2013. [Online]. Available: http://www.opticsexpress.org/abstract.cfm?URI=oe-21-7-9103

[10] S. Dey and S. Mandal, "Modeling and analysis of quadruple optical ring resonator performance as optical filter using Vernier principle," *Opt. Commun.*, vol. 285, no. 4, pp. 439–446, Feb. 2012. [Online]. Available: http://www.sciencedirect.com/science/article/pii/S0030401811010819

[11] O. Schwelb, "The nature of spurious mode suppression in extended FSR microring multiplexers," *Opt. Commun.*, vol. 271, no. 2, pp. 424–429, Mar. 2007.

[12] C. Chaichuay, P. P. Yupapin, and P. Saeung, "The serially coupled multiple ring resonator filters and Vernier effect," *Opt. Appl.*, vol. 39, no. 1, pp. 175–194, Mar. 2009.

[13] Y. Goebuchi, T. Kato, and Y. Kokubun, "Optimum arrangement of high-order series-coupled microring resonator for crosstalk reduction," *Jpn. J. Appl. Phys.*, vol. 45, no. 7, pp. 5769–5774, Jul. 2006. [Online]. Available: http://jjap.jsap.jp/link?JJAP/45/5769/

[14] D. Zhang, Y. Huang, X. Ren, X. Duan, B. Shen, Q. Wang, X. Zhang, and S. Cai, "Add–drop filters based on asymmetric high-order microring resonators," in *Proc. SPIE*, Nov. 2012, vol. 8555, pp. 85550U-1–85550U-7. [Online]. Available: http://dx.doi.org/10.1117/12.999382

[15] O. Schwelb and I. Frigyes, "Vernier operation of series-coupled optical microring resonator filters," *Microw. Opt. Technol. Lett.*, vol. 39, no. 4, pp. 257–261, Nov. 2003. [Online]. Available: http://onlinelibrary.wiley.com/doi/10.1002/mop.11185/abstract

[16] R. Boeck, J. Flueckiger, H. Yun, L. Chrostowski, and N. A. F. Jaeger, "High performance Vernier racetrack resonators," *Opt. Lett.*, vol. 37, no. 24, pp. 5199–5201, Dec. 2012. [Online]. Available: http://ol.osa.org/abstract.cfm?URI=ol-37-24-5199

[17] Y. Yanagase, S. Suzuki, Y. Kokubun, and S. T. Chu, "Box-like filter response and expansion of FSR by a vertically triple coupled microring resonator filter," *J. Lightwave Technol.*, vol. 20, no. 8, pp. 1525–1529, Aug. 2002.

[18] M. Mancinelli, R. Guider, P. Bettotti, M. Masi, M. R. Vanacharla, J. Fedeli, D. V. Thourhout, and L. Pavesi, "Optical characterization of silicon-on-insulator-based single and coupled racetrack resonators," *J. Nanophoton.*, vol. 5, no. 1, pp. 051705-1–051705-8, Jun. 2011.

[19] K. Oda, N. Takato, and H. Toba, "A wide-FSR waveguide double-ring resonator for optical FDM transmission systems," *J. Lightwave Technol.*, vol. 9, no. 6, pp. 728–736, Jun. 1991.

[20] S. Suzuki, K. Oda, and Y. Hibino, "Integrated-optic double-ring resonators with a wide free spectral range of 100 GHz," *J. Lightwave Technol.*, vol. 13, no. 8, pp. 1766–1771, Aug. 1995.

[21] Y. Goebuchi, T. Kato, and Y. Kokubun, "Expansion of tuning range of wavelength selective switch using Vernier effect of series coupled microring resonator," in *Proc. 18th Annu. Meet. IEEE LEOS*, Oct. 2005, pp. 734–735.

[22] R. Boeck, N. A. F. Jaeger, N. Rouger, and L. Chrostowski, "Series-coupled silicon racetrack resonators and the Vernier effect: Theory and measurement," *Opt. Exp.*, vol. 18, no. 24, pp. 25 151–25 157, Nov. 2010. [Online]. Available: http://www.opticsexpress.org/abstract.cfm?URI=oe-18-24-25151

[23] F. Boffi, L. Bolla, P. Galli, S. Ghidini, and L. Socci, "Method and device for tunable optical filtering using Vernier effect," Eur. Union Patent EP2 181 348 B1, Jan. 18, 2012.

[24] H. Yan, X. Feng, D. Zhang, and Y. Huang, "Integrated optical add–drop multiplexer based on a compact parent-sub microring-resonator structure," *Opt. Commun.*, vol. 289, pp. 53–59, Feb. 2013. [Online]. Available: http://www.sciencedirect.com/science/article/pii/S003040181201067X

[25] T. Claes, W. Bogaerts, and P. Bienstman, "Experimental characterization of a silicon photonic biosensor consisting of two cascaded ring resonators based on the Vernier-effect and introduction of a curve fitting method for an improved detection limit," *Opt. Exp.*, vol. 18, no. 22, pp. 22747–22761, Oct. 2010. [Online]. Available: http://www.opticsexpress.org/abstract.cfm?URI=oe-18-22-22747

[26] J. Hu and D. Dai, "Cascaded-ring optical sensor with enhanced sensitivity by using suspended Si-nanowires," *IEEE Photon. Technol. Lett.*, vol. 23, no. 13, pp. 842–844, Jul. 2011.

[27] L. Jin, M. Li, and J.-J. He, "Highly-sensitive silicon-on-insulator sensor based on two cascaded micro-ring resonators with Vernier effect," *Opt. Commun.*, vol. 284, no. 1, pp. 156–159, Jan. 2011. [Online]. Available: http://www.sciencedirect.com/science/article/pii/S0030401810008904
[28] X. Jiang, "Silicon nanowire waveguide sensor based on two cascaded ring resonators," presented at the Asia Communications Photonics Conf., Guangzhou, China, Nov. 2012, Optical Society of America, Paper AS4E.3. [Online]. Available: http://www.opticsinfobase.org/abstract.cfm?URI=ACP-2012-AS4E.3
[29] T. Chu, N. Fujioka, and M. Ishizaka, "Compact, lower-power-consumption wavelength tunable laser fabricated with silicon photonic-wire waveguide micro-ring resonators," *Opt. Exp.*, vol. 17, no. 16, pp. 14063–14068, Aug. 2009. [Online]. Available: http://www.opticsexpress.org/abstract.cfm?URI=oe-17-16-14063
[30] P. Rabiei and W. H. Steier, "Tunable polymer double micro-ring filters," *IEEE Photon. Technol. Lett.*, vol. 15, no. 9, pp. 1255–1257, Sep. 2003.
[31] W. Shi, X. Wang, W. Zhang, H. Yun, C. Lin, L. Chrostowski, and N. A. F. Jaeger, "Grating-coupled silicon microring resonators," *Appl. Phys. Lett.*, vol. 100, no. 12, pp. 121118-1–121118-4, Mar. 2012.
[32] P. Orlandi, P. Velha, M. Gnan, P. Bassi, A. Samarelli, M. Sorel, M. J. Strain, and R. De La Rue, "Microring resonator with wavelength selective coupling in SOI," in *Proc. 8th Int. Conf. Group IV Photon.*, London, U.K., Sep. 2011, pp. 281–283.
[33] W. Shi, H. Yun, C. Lin, M. Greenberg, X. Wang, Y. Wang, S. T. Fard, J. Flueckiger, N. A. F. Jaeger, and L. Chrostowski, "Ultra-compact, flat-top demultiplexer using anti-reflection contra-directional couplers for CWDM networks on silicon," *Opt. Exp.*, vol. 21, no. 6, pp. 6733–6738, Mar. 2013. [Online]. Available: http://www.opticsexpress.org/abstract.cfm?URI=oe-21-6-6733
[34] W. Bogaerts, R. Baets, P. Dumon, V. Wiaux, S. Beckx, D. Taillaert, B. Luyssaert, J. Van Campenhout, P. Bienstman, and D. Van Thourhout, "Nanophotonic waveguides in silicon-on-insulator fabricated with CMOS technology," *J. Lightw. Technol.*, vol. 23, no. 1, pp. 401–412, Jan. 2005.
[35] W. Shi, X. Wang, W. Zhang, L. Chrostowski, and N. A. F. Jaeger, "Contradirectional couplers in silicon-on-insulator rib waveguides," *Opt. Lett.*, vol. 36, no. 20, pp. 3999–4001, Oct. 2011. [Online]. Available: http://ol.osa.org/abstract.cfm?URI=ol-36-20-3999
[36] D. Minoli, *Telecommunications Technology Handbook*. Norwood, MA, USA: Artech House, Sep. 2003.
[37] "ITU-T G.671 Transmission characteristics of optical components and subsystems," Tech. Rep., Feb. 2012.
[38] "ITU-T G.692 Optical interfaces for multichannel systems with optical amplifiers," Tech. Rep., Oct. 1998.
[39] *DWDM and CWDM Three Port Device Optical Parameter Definition and Test Requirements*, Alliance Fiber Optic Products, Inc., Sunnyvale, CA, USA, 2003.
[40] R. J. Bojko, J. Li, L. He, T. Baehr-Jones, M. Hochberg, and Y. Aida, "Electron beam lithography writing strategies for low loss, high confinement silicon optical waveguides," *J. Vac. Sci. Technol. B*, vol. 29, no. 6, pp. 06F309-1–06F309-6, Oct. 25, 2011. [Online]. Available: http://link.aip.org/link/?JVB/29/06F309/1
[41] *Optical Add/Drop Multiplexers 100 GHz OADM (1x2)*, Photonics-USA, Bothell, WA, USA.
[42] *Fiber Optic DWDM Single Add/Drop Device*, AOXC Technologies, Taipei, Taiwan.